Short Papers

Mechanical Filtering Effect of Elastic Cover for Tactile Sensor

Makoto Shimojo

***Abstract*—Tactile sensors are ordinarily covered with an elastic cover to protect the sensor from being damaged by shock or chemical contamination. The cover, however, greatly decreases the sensor's spatial resolution. This effect becomes serious in the fabrication of a high-spatial-resolution sensor, even if the cover is only 0.2 mm thick, when the sensor requires a spatial resolution of less than 1 mm. This paper analyzes the low-pass spatial filtering effect of the cover, calculates the filtering gain for different types of elastic cover materials using the finite-element method, and gives preliminary experimental results.**

***Index Terms*—Cover materials, filtering effect, spatial resolution, tactile sensor.**

I. Introduction

Tactile sensors are ordinarily covered with an elastic cover to protect the sensor from being physically damaged by shock or chemically contaminated by oil and other materials. The soft elastic cover also has advantages. A robot hand with a sensor covered by a soft material can, for example, holds an object easily because the contact area is comparatively wide and the friction between the sensor and the object is increased.

The state of stress distribution on the underlying sensing elements changes, however, due to the elastic cover because of the cover's mechanical filtering effect. This effect has not been considered so much, and the pitch of the sensing elements is sometimes regarded as the spatial resolution of the tactile sensor.

Fearing, Hollerbach, and Nicolson studied basic solid mechanics for an elastic material, developing a two-dimensional model and analyzing the mechanical spatial filtering effect of an incompressible and homogeneous elastic medium [1]–[4]. Speeter analyzed three-dimensional stress and strain tensors with elastic layers covering tactile sensors [5]. Cameron *et al*. also used a three-dimensional model for reconstructing a surface pressure profile for a static tactile image [6]. Ricker and Ellis also analyzed the normal and the shear strain for an annular tactile sensor using the finite-element method (FEM) [7]. Few attempts have been made, however, at quantifying the mechanical filtering effect of the cover as this relates to the parameters of the elastic material, such as thickness, the Young's modulus, and the Poisson's ratio.

We analyzed the mechanical spatial filtering effect of elastic materials and determined the relationship between spatial filter gain and the properties of the elastic material. The elastic cover exhibits a low-pass spatial filtering effect, its characteristics changing with cover material parameters as described above. It is important to clarify its characteristics in fabricating a high-spatial-resolution tactile sensor [8], [9]. We therefore analyzed the mechanical filtering effect and calculated the filter gain for the elastic cover materials.

Manuscript received January 2, 1995; revised August 1, 1995. This paper was recommended for publication by Associate Editor R. Howe and Editor S. E. Salcudean upon evaluation of the reviewers' comments.

The author is with the Informational Factors Laboratory, Human-Environment System Department, National Institute of Bioscience and Human-Technology, Tsukuba, Ibaraki 305, Japan.

Publisher Item Identifier S 1042-296X(97)01050-1.

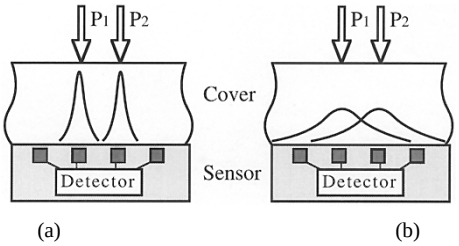

Fig. 1. Pressure distribution interference under the elastic cover. (a) Pressure pattern separated. (b) Pressure pattern overlapped.

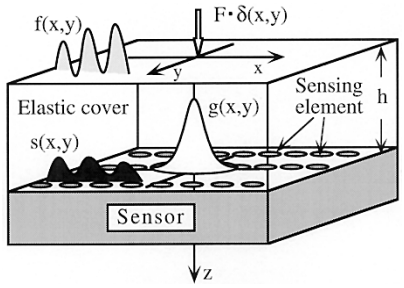

Fig. 2. Pressure distribution under the elastic cover caused by the point load.

II. Theoretical Analysis of Spatial Filtering Effect Due to the Elastic Cover

Fig. 1 shows the stress distribution under the cover caused by two concentrated loads. In Fig. 1(a), the pressure distributions for P_1 and P_2 were separated. In Fig. 1(b), they were overlapped. This overlap decreases the sensor's spatial resolution. This effect is a serious factor in the fabrication of a sensor that requires a high spatial resolution. It is therefore important to determine this effect and cover material selection criteria to fabricate a high-spatial-resolution sensor. The spatial filtering effect of the cover is analyzed theoretically in the sections that follow.

As shown in Fig. 2, the stress distribution under an elastic cover is assumed to be $g(x, y)$, on whose surface point load $F \cdot \delta(x, y)$ is applied. Stress distribution $s(x, y)$ under the cover is expressed by (1) as the convolution of stress distribution $f(x, y)$ on the surface of the cover and $g(x, y)$:

$$s(x, y) = \iint g(\xi, \eta) f(x - \xi, y - \eta)\, d\xi\, d\eta. \tag{1}$$

Applying a Fourier transformation yields (2):

$$S(u, v) = G(u, v) * F(u, v) \tag{2}$$

Result $G(u, v)$ is the spatial filter gain of the cover. Spatial frequency $F(u, v)$ of pressure distribution on the cover surface multiplied by $G(u, v)$ corresponds to spatial frequency $S(u, v)$ on the sensing elements of the sensor.

Thus, by obtaining $g(x, y)$ and calculating $G(u, v)$, we can analyze the spatial filter gain due to the cover. Filter gain $G(u, v)$ is the Fourier transformation of $g(x, y)$, which is a circular symmetrical

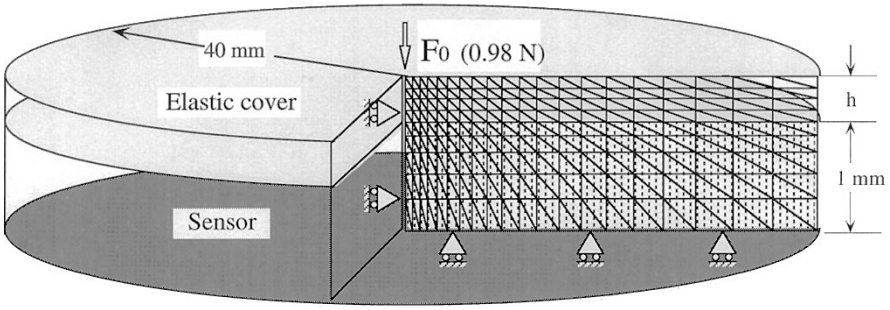

Fig. 3. Finite-element model. 18 elements in the direction of thickness. 20 elements in the direction of radius.

function. Filter gain $G(u, v)$ is thus also circularly symmetrical, and the two-dimensional Fourier transform becomes a Hankel transformation expressed as

$$G(q) = \int_{-\infty}^{\infty}\int_{-\infty}^{\infty} g(x,y)e^{-i2\pi(xu+yv)}\,dx\,dy = 2\pi\int_{-\infty}^{\infty} g(r)J_0(2\pi rq)r\,dr \quad (3)$$

where $J_0(z)$ represents the Bessel function of the first type

$$J_0(z) = \frac{1}{2\pi}\int_0^{2\pi} e^{-iz\cos\beta}\,d\beta \quad (r^2 = x^2 + y^2, q^2 = u^2 + v^2). \quad (4)$$

III. Calculation of the Spatial Filter Gain of the Cover

It is difficult to calculate $g(x, y)$ when the cover and the sensor's Young's modulus, and Poisson's ratio are different. So we used FEM to calculate $g(x, y)$ for each cover material.

A. FEM for Calculating the Stress Distribution

Stress distribution $g(x, y)$ in three-dimensional space shown in Fig. 2, is symmetrical to the z axis. In such a case, the FEM algorithm for the two-dimensional space can be used. We used Togawa's FEM algorithm for the calculation [10], with triangular elements used for the FEM element as shown in Fig. 3. There are 18 elements in the direction of thickness, and 20 elements in the direction of radius, for a total 360 elements. The sensor is 1 mm thick, with 10 elements in the direction of thickness. The cover is assumed to be 0.1, 0.2, 0.4, and 0.6 mm thick, with 8 elements in the direction of thickness. Stress distribution changes rapidly near the loading point, so elements there must be small, about 0.05 mm, becoming larger with increasing distance. The FEM model is 40 mm in diameter. Because the stress distribution of elements near the edge of the FEM model becomes negligible, it is calculated results from the FEM. This diameter is sufficiently accurate for practical purposes. The concentrated load (0.98 N) is applied as shown in Fig. 3.

B. Calculating the Spatial Filter Gain

We used three parameters for the cover material—thickness, the Young's modulus, and the Poisson's ratio—to calculate the spatial filter gain.

1) Effects of Cover Thickness: Calculation was conducted by changing the thickness of the cover. The Young's modulus of the sensor was set at 980 MPa and that of the cover at 98 MPa. The Poisson's ratio was 0.3 for both materials. It was assumed that the sensor was a flexible printed-circuit film and the cover was soft polyethylene film. The cover thickness was set at 0.1, 0.2, 0.4, and 0.6 mm for the calculation. Fig. 4 shows stress distribution results. As these results make clear, stress distribution $g(x, y)$ broadened and its peak became lower in inverse proportion to the square of the thickness.

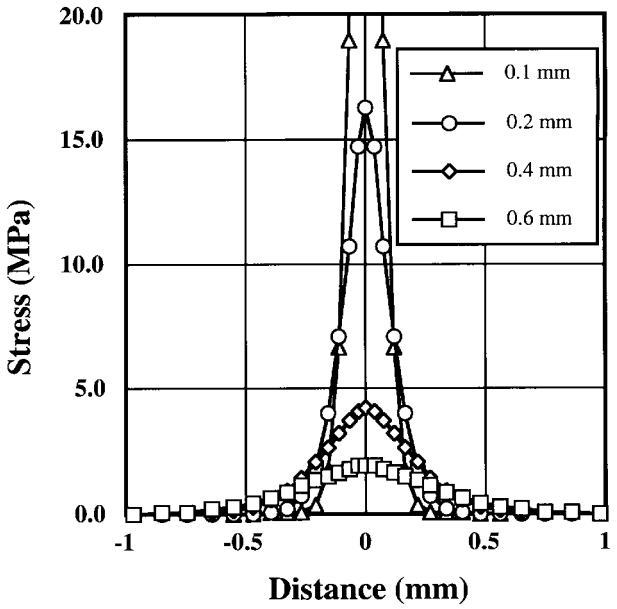

Fig. 4. Difference in stress distribution$g(r)$ with the thickness of the cover.

Fig. 5 shows calculated spatial filter gain $G(q)$. Filter gains at spatial frequency 1 mm^{-1} are 0.9 for a cover 0.1 mm thick, 0.8 for one 0.2 mm thick, 0.4 for one 0.6 mm thick, and 0.2 for one 1.0 mm thick. The gain decreased rapidly with the increasing cover thickness. The spatial filter gain at a spatial frequency of 2 mm^{-1} was nearly zero for a cover 0.4 mm thick, and was 0.4 even for a cover 0.2 mm thick. This means that the spatial resolution of the tactile sensor depended on the thickness of the cover as well as he pitch of the sensing element. In other words, the spatial resolution of the tactile sensor depended strongly on the thickness of the cover.

2) Effects of the Cover's Young's Modulus: Calculation was conducted changing the Young's modulus of the cover, which was set at 98, 490, 980, 4903, and 9807 MPa for calculations, assuming that the cover was made of materials ranging from soft polyethylene film to phenolic resin. The Young's modulus of the sensor was set at 980 MPa, the Poisson's ratio at 0.3, and the thickness of the cover at 0.2 mm.

Fig. 6 shows calculated spatial filter gain $G(q)$. These results make it clear that the softer the cover, the better the spatial filter gain. No great difference was found in the spatial filter gain, even when the Young's modulus of the cover material was one-tenth that of the sensor.

3) Effects of the Cover's Poisson's Ratio: Calculation was conducted changing the Poisson's ratio of the cover. The Poisson's ratios were set at 0.2, 0.3, 0.4, and 0.45; the Young's modulus of the sensor was set at 980 MPa, and the Poisson's ratio was set at 0.3. The Young's modulus of the cover was set at 98 MPa; and the

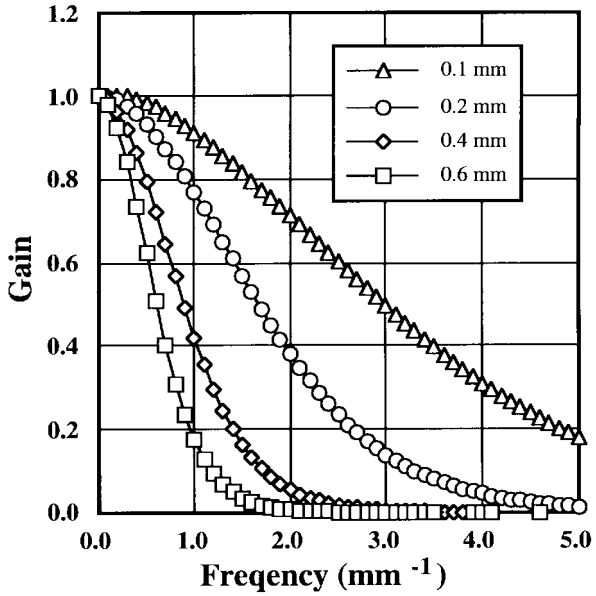

Fig. 5. Difference in spatial filter gain with the thickness of the cover material.

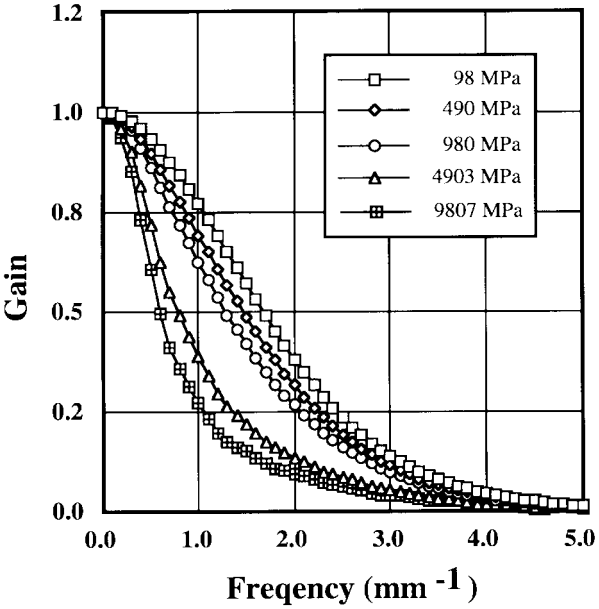

Fig. 6. Difference in spatial filter gain with the Young's modulus of the cover material.

thickness was set to 0.2 mm, assuming that the sensor was flexible printed-circuit film and the cover of soft polyethylene film.

Fig. 7 shows calculated filter gain $G(q)$. A slight difference was observed among the results, with a high Poisson's ratio giving more favorable results.

IV. Calculated Pressure Patterns Under the Cover

Fig. 8 shows the calculated pressure pattern under the cover with changing the thickness, the Young's modulus and the Poisson's ratio of the elastic cover. Fig. 8(a) shows the original pattern on the cover. The pattern was a square ring 1.0 mm long on the outside and 0.6 mm on the inside, constructed from 40 × 40 matrix array elements, each 0.05 mm long. Fig. 8(b) shows the sensor covered with a elastic cover. Fig. 8(c) shows the cross section of the pressure distribution

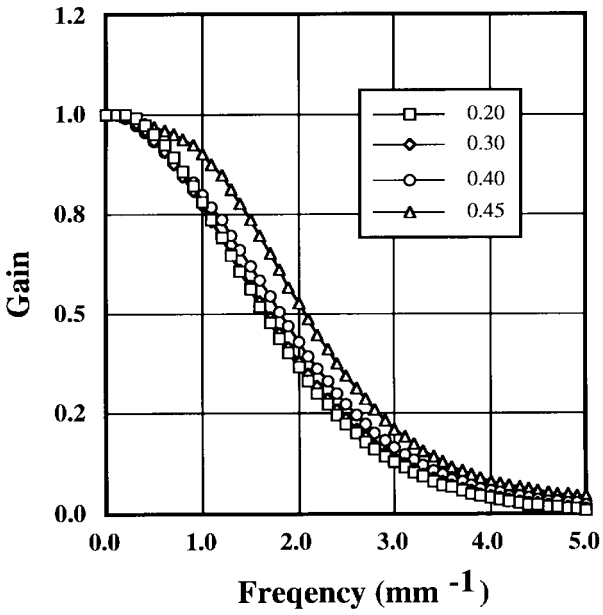

Fig. 7. Difference in spatial filter gain with the Poisson's ratio of the cover material.

under the cover, where the cover's thickness is 0.2 mm, the Young's modulus is 98 MPa and the Poisson's ratio is 0.3.

Fig. 8(d) shows the results where the parameter of thickness was changed. The pressure pattern is close to that of the original pattern where the cover was 0.1 mm thick. In the case where the cover was 0.2 mm thick as shown in Fig. 8(c), corner enhancement was observed, but the pattern differs little from that of the original. For a 0.4 mm thickness, the peak of the pattern became lower and the pattern profile was broader. For a 0.6 mm thickness, the profile of the pattern was spread and the inner hole pattern was dim and it was difficult to determine the original pattern. In such a case, deconvolution is useful in estimating the original pattern. Some papers have dealt with this technique [11], [12], [6]. But its estimated accuracy depends greatly on the sensitivity and spacing density of sensing elements. This point will present an interesting area of future study.

In results where the parameter of the Young's modulus was changed from that in Fig. 8(c) to that in Fig. 8(e), the pressure pattern under the cover did not change much if the cover was softer than that of the sensor. The pattern differs greatly, however, when the Young's modulus of the cover became 4903 MPa. Its Young's modulus was five times harder than that of the sensor.

When the parameter of the Poisson's ratio was changed from that in Fig. 8(c) to that in Fig. 8(f), the patterns differ slightly.

V. Experiments

Experiments were conducted to determine stress distribution $g(x, y)$, then experimental and calculated results were compared. Fig. 9 shows the measuring device. Silicon-gage pressure detectors 4.57 mm square were arranged one-dimensionally on a flat table. Three types of silicon rubber sheet—0.25, 0.5, and 1.0 mm thick—were tested. A concentrated load was applied using a steel rod with a rounded tip having a radius of 3 mm. A concentrated load (0.98N) was applied vertically to the cover, and the loading position was changed inch by inch to measure the relationship between the loading position and the output of load cells.

Fig. 10 shows the relationship between experimental and anticipated values. The anticipated value was that estimated for the total load of stress distribution on the load cell, where the stress distribution

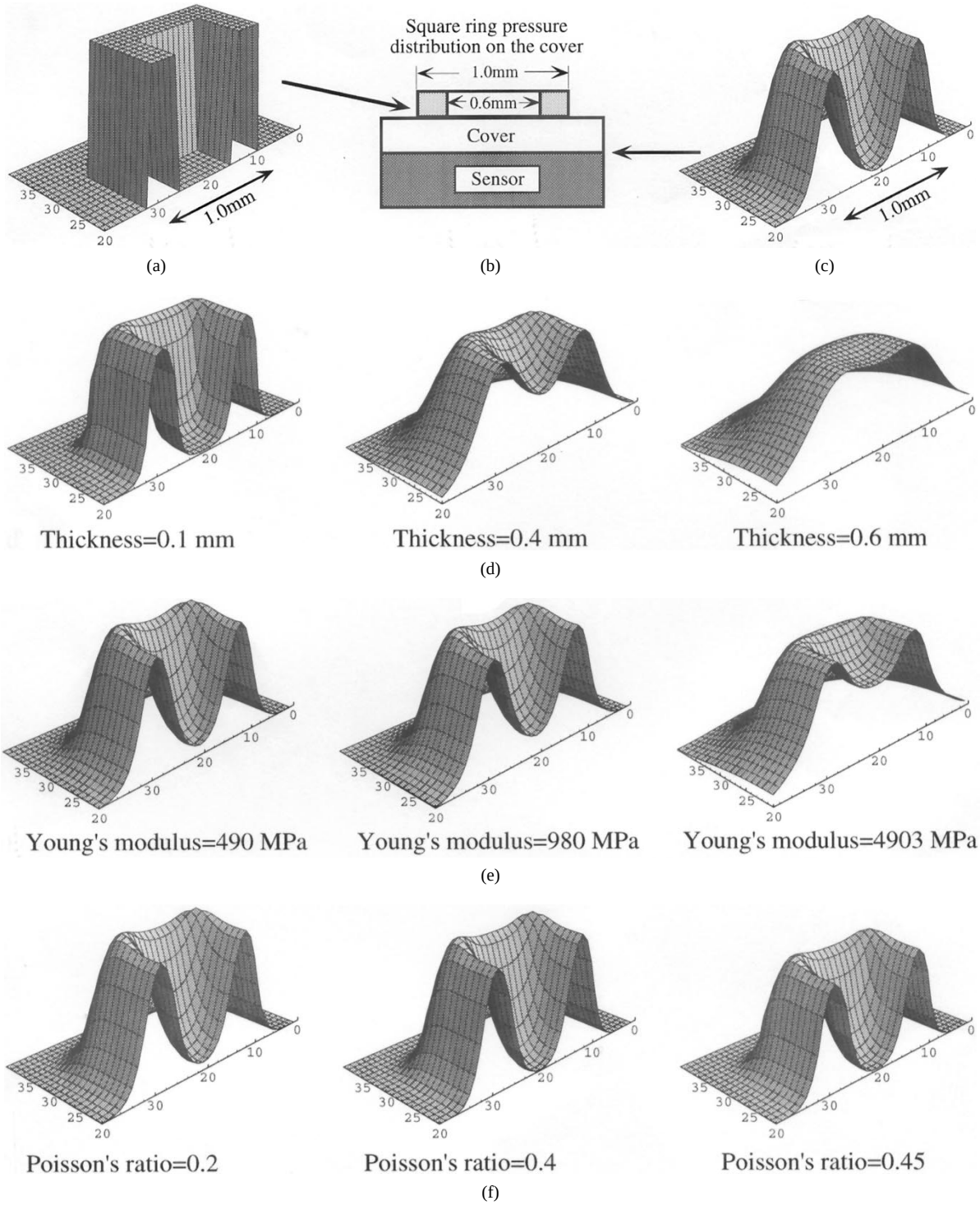

Fig. 8. Stress distribution under the cover with changing thickness, Young's modulus, and Poisson's ratio of the cover. (a) Pressure distribution on the cover. (b) Sensor: Thickness (1.0 mm), Poisson's ratio (0.3), Young's modulus (980 MPa). (c) Pressure distribution under the cover. (d) Thickness. (e) Young's modulus. (f) Poisson's ratio.

was calculated from $g(x, y)$. For the calculation, it was used that the Young's modulus of the cover was 98 MPa and the Poisson's ratio was 0.3. Solid lines indicate anticipated values. Squares, circles, and triangles are experimental results. Experimental values agree well with anticipated results.

VI. Conclusions

We have analyzed the mechanical spatial filtering effect of an elastic cover and calculated the spatial filter gain for different types of elastic cover materials. The results made it clear that, even if the elastic cover is only 0.2 mm thick, the spatial filter gain at a spatial frequency of 2 mm^{-1} becomes less than 0.4, and spatial filtering effect cannot be neglected. This effect is especially serious in the fabrication of tactile sensors of less than 1 mm having a spatial resolution.

1) The spatial resolution of the tactile sensor is determined by the thickness of the cover as well as the pitch of the sensing elements beneath the cover.

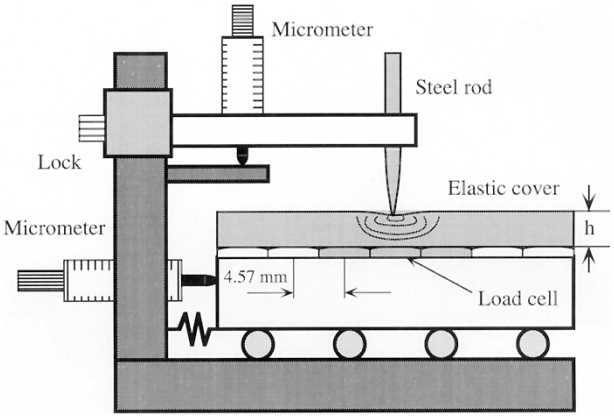

Fig. 9. Test device for measuring stress distribution under the cover.

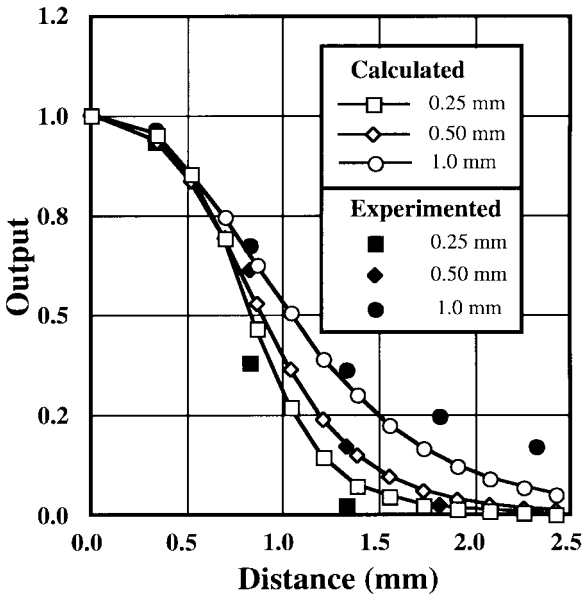

Fig. 10. Experimental results: measured and anticipated values.

2) A softer material provides a better cover, but no great difference was observed in the spatial filter gain even when the Young's modulus of the cover material is one-tenth that of the sensor.
3) A material with a higher Poisson's ratio is better, but the difference is only a slight one.

ACKNOWLEDGMENT

The author would like to thank O. Okuda for his invaluable advice on FEM use.

REFERENCES

[1] R. S. Fearing and J. M. Hollerbach, "Basic solid mechanics for tactile sensing," *Int. J. Robot. Res.*, vol. 4, no. 3, pp. 40–54, 1985.
[2] R. S. Fearing, "Tactile sensing mechanisms," *Int. J. Robot. Res.*, vol. 9, no. 3, pp. 3–23, 1990.
[3] E. J. Nicolson and R. S. Fearing, "Sensing capability of linear elastic cylindrical fingers," in *Proc. 1993 IEEE/RSJ Int. Conf. Intelligent Robot. Syst.*, Yokohama, 1993, pp. 178–185.
[4] R. S. Fearing, "Tactile sensing, perception and shape interpretation," Ph.D. dissertation, Stanford Univ., CA, Dec. 1987.
[5] T. H. Speeter, "Three-dimensional finite element analysis of elastic continua for tactile sensing," *Int. J. Robot. Res.*, vol. 11, no. 1, pp. 1–19, 1990.
[6] A. Cameron, R. Daniel, and H. Durrant-Whyte, "Touch and motion," in *Proc. Int. Conf. Robot. Automat.*, Philadelphia, PA, 1988, pp. 1062–1067.
[7] S. L. Ricker and R. E. Ellis, "2-D finite-element models of tactile sensors," in *Proc. Int. Conf. Robot. Automat.*, Atlanta, GA, 1993, pp. 941–947.
[8] W. E. Hillis, "A high resolution imaging touch sensor," *Int. J. Robot. Res.*, vol. 1, no. 2, pp. 33–44, 1982.
[9] M. Shimojo, M. Ishikawa, and K. Kanaya, "A flexible high resolution tactile imager with video signal output," in *Proc. Int. Conf. Robot. Automat.*, Sacramento, CA, 1991, pp. 384–391.
[10] H. Togawa, "A book for FEM," Baifu-kan, p. 219, 1981.
[11] G. Canepa *et al*., "Shape from touch by a neural net," in *Proc. 1992 IEEE Int. Conf. Robot. Automat.*, Nice, 1992, pp. 2075–2080.
[12] D. De Rossi, A. Caiti, R. Bianchi, and G. Canepa, "Fine-form tactile discrimination though inversion of data from a skin-like sensor," in *Proc. 1991 IEEE Int. Conf. Robot. Automat.*, Sacramento, CA, 1991, pp. 398–403.
[13] M. Shimojo, "Spatial filtering characteristics of an elastic cover for a tactile sensor," *Trans. JSME (C)*, vol. 59, no. 567, pp. 3458–3463, 1993.

Autonomous Mobile Robot Global Motion Planning and Geometric Beacon Collection Using Traversability Vectors

Jason A. Janét, Ren C. Luo, and Michael G. Kay

***Abstract*—Approaches in global motion planning (GMP) and geometric beacon collection (for self-localization) using traversability vectors have been developed and implemented in both computer simulation and actual experiments on mobile robots. Both approaches are based on the same simple, modular, and multifunctional traversability vector (t-vector). Through implementation it has been found that t-vectors reduce the computational requirements to detect path obstructions, Euclidean optimal via points, and geometric beacons, as well as to identify which features are visible to sensors. Environments can be static or dynamic and polygons are permitted to overlap (i.e., intersect or be nested). While the t-vector model does require that polygons be convex, it is a much simpler matter to decompose concave polygons into convex polygon sets than it is to require that polygons not overlap, which is required for many other GMP models. T-vectors also reduce the data size and complexity of standard V-graphs and variations thereof. This paper presents the t-vector model so that the reader can apply it to mobile robot GMP and self-localization.**

***Index Terms*—Computational geometry collision detection, geometric beacon detection/collection, mobile robot, motion planning, range senor prediction, self-localization.**

Manuscript received September 17, 1994; revised June 15, 1995. This work was presented at the IEEE International Conference on Robotics and Automation, Nagoya, Japan, May 1995. This paper was recommended for publication by Associate Editor R. Chatila and Editor S. E. Salcudean upon evaluation of the reviewers' comments.

The authors are with the Center for Robotics and Intelligent Machines, Department of Electrical and Computer Engineering, North Carolina State University, Raleigh, NC 27695 USA.

Publisher Item Identifier S 1042-296X(97)01035-5.